The structure of mesoporous silica obtained by pseudomorphic transformation of SBA-15 and SBA-16

Nicola Zucchetto[a], Michael J. Reber[a], Lias Pestalozzi[a], Ramon Schmid[b,c], Antonia Neels[c], Dominik Brühwiler[a,*]

* Corresponding Author. E-mail: dominik.bruehwiler@zhaw.ch

[a] Institute of Chemistry and Biotechnology, Zürich University of Applied Sciences (ZHAW), CH-8820 Wädenswil, Switzerland.

[b] Empa, Swiss Federal Laboratories for Materials Sciences and Technology, Laboratory for Biomimetic Membranes and Textiles, CH-9014 St. Gallen, Switzerland.

[c] Empa, Swiss Federal Laboratories for Materials Sciences and Technology, Center for X-ray Analytics, CH-8600 Dübendorf, Switzerland.

Microporous Mesoporous Mater. 257 (2018) 232 – 240

Abstract

Mesoporous silica with bimodal pore size distributions was prepared by pseudomorphic transformation of SBA-15 and SBA-16 in the presence of hexadecyltrimethylammonium ions as a structure-directing agent. The characteristic particle morphology of the starting materials was retained after the transformation. Analysis of the products by gas sorption and small-angle X-ray scattering (SAXS) revealed hybrid pore structures, which featured – depending on the degree of transformation – variable contributions from the original and the newly introduced pore systems. In the case of SBA-15, it was found that a high degree of transformation leads to a seemingly complete conversion of the original pores with a diameter of 7.1 nm to pores with a diameter of 4.0 nm. The SAXS pattern of the product shows additional peaks that can be assigned to the original SBA-15 pore spacing. Similarly, a cubic phase could be observed in the samples prepared by pseudomorphic transformation of SBA-16, despite an almost complete conversion of the SBA-16 cavities. This leads to the conclusion that the pore structure of the starting material significantly affects the outcome of the pseudomorphic transformation, thus opening possibilities for the synthesis of new porous materials with complex pore systems.

Keywords: Bimodal mesoporous silica; Hybrid pore structure; Pseudomorphic transformation; Cavitation; Bottleneck.

1. Introduction

In terms of research activity, materials of the M41S [1,2] and SBA families [3,4] are the most prominent types of ordered mesoporous silica. Catalysis [5], chromatography [6], organization of molecular guests [7], environmental remediation [8], and drug delivery [9] are some of the fields where these materials can find potential application. While considerable progress regarding the engineering of the pore size and the introduction of functional groups has been made [10-12], much less emphasis has been put on the control of the particle size and shape for a specific application. The simultaneous control of the pore size, pore structure, particle size, particle shape, and surface functional groups poses a challenge.

An elegant way to alter the pore size of a mesoporous material without affecting its particle size and shape was proposed by Martin et al. [13]. This so-called pseudomorphic transformation pathway uses a structure-directing agent (SDA) to rearrange the pore system of a preformed macroporous material. Functional groups can be introduced during the transformation and the pore size can be adjusted to a certain degree by using differently sized SDAs [14]. MCM-41 type silica tubes [15] and monodisperse magnetic mesoporous silica microspheres [16] have been prepared by pseudomorphic transformation of silica shells deposited onto hard templates. Pseudomorphic transformation can also be applied to millimeter-sized silica spheres [17] or to an ordered mesoporous material such as SBA-15, thus converting its pore system into a MCM-41 type structure [18]. Bimodal mesoporous materials with two well-defined pore size regimes have been prepared by carefully balancing the degree of pseudomorphic transformation. Partial pseudomorphic transformation was shown to alter the structure of the porous starting material from the outside to the inside, thus virtually creating a shell with a reduced pore size. The pH thereby governs the equilibrium between dissolution and reprecipitation of the silica matrix [18].

Based on these previous results we can make the general conclusion that the partial pseudomorphic transformation of SBA-15 in the presence of hexadecyltrimethylammonium bromide (CTAB) yields a

material consisting of two types of pore size domains, one originating from the SBA-15 starting material, and the other being formed by a rearrangement of the original pore structure in the presence of the SDA. The question remains whether this newly introduced pore structure can in fact be considered as a true MCM-41 type structure, i.e., a hexagonal arrangement of one-dimensional pores. Furthermore, the role of the original pore structure in determining the structure of the newly introduced domains is unclear. We have therefore investigated the partial pseudomorphic transformation of SBA-15 (one-dimensional pore structure, space group $P6mm$) and of SBA-16 (three-dimensional pore structure, space group $Im\bar{3}m$) in the presence of CTAB. Analysis by argon sorption and small angle X-ray scattering (SAXS) revealed that the transformed materials contain various domains and retain some of the structural features of the SBA type starting materials. In all cases, the particle morphology and average particle size remained unaltered after transformation and did not reflect the reorganization of the pore structure.

2. Experimental

2.1. Materials

Pluronic P123, Pluronic F127, tetraethyl orthosilicate (TEOS, ≥ 99 %), sodium hydroxide (97 %), aqueous ammonia (25 %), and hydrochloric acid (32 %) were obtained from Sigma-Aldrich. Pluronic P123 and F127 are triblock poly(ethylene oxide)–poly(propylene oxide)–poly(ethylene oxide) ($EO_xPO_yEO_x$) copolymers, with x = 20 and y = 70 for P123, and x = 106 and y = 70 for F127. Hexadecyltrimethylammonium bromide (CTAB, 99+ %) was obtained from Acros. All chemicals were used as received. Previously published procedures were followed to prepare the parent materials SBA-15 [3], MCM-41 [19], and SBA-16 [20]. Details on the syntheses are given below.

2.2. Synthesis of SBA-15

An amount of 2.2 g of P123 was dissolved in 80 mL of 1.55 M hydrochloric acid. Once a clear solution was obtained, 5 mL of TEOS was slowly added. The mixture was stirred for 20 h at 35 °C, transferred to a Teflon-lined autoclave, and placed in a preheated oven at 100 °C for 24 h. The autoclave was allowed to cool to room temperature before the product was recovered by filtration and washing with at least 1 L of H_2O. The material was allowed to dry at room temperature overnight and then calcined in air at 550 °C for 12 h. A heating rate of 2 °C min^{-1} was applied.

2.3. Synthesis of MCM-41

An amount of 2.2 g of CTAB was dissolved in a solution of 52 mL of H_2O and 25 mL of aqueous ammonia (25 %). After dropwise addition of 10 mL of TEOS, the mixture was stirred at room temperature for 3 h. It was then transferred to a Teflon-lined autoclave and put in an oven at 110 °C for 48 h. The autoclave was allowed to cool to room temperature before the product was recovered by filtration and washing with at least 250 mL of H_2O. The material was allowed to dry at room temperature overnight. The SDA was removed by heating at 300 °C for 2 h and subsequent calcination at 550 °C for 12 h. A heating rate of 2 °C min^{-1} was applied.

2.4. Synthesis of SBA-16

An amount of 0.47 g of F127 and 55 mg of CTAB was dissolved in 65 mL of 0.4 M hydrochloric acid. Once a clear solution was obtained, 1.66 mL of TEOS was added under strong stirring. The mixture was stirred for 30 minutes at room temperature, transferred to a Teflon-lined autoclave, and placed in a preheated oven at 95 °C for 120 h. The autoclave was allowed to cool to room temperature before the product was

recovered by filtration and washing with 5 mL of H_2O. The material was allowed to dry at room temperature overnight and then calcined in air at 550 °C for 12 h. A heating rate of 2 °C min^{-1} was applied.

2.5. Pseudomorphic Transformation

An amount of 300 mg of the parent silica (SBA-15 or SBA-16) was mixed with 182 mg of CTAB and a varying amount of NaOH. The ratio of the mass of silica (m_{silica}) and NaOH (m_{NaOH}) for each synthesis is given in Table 1 (SBA-15) and Table 2 (SBA-16). To this mixture, 2 mL of H_2O was added and stirred for 30 min in a Teflon liner, which was then placed in an autoclave (100 mL volume) and heated in an oven at 100 °C for 6 h. After allowing the autoclave to cool to room temperature, the product was filtered, washed with 250 mL of H_2O, and calcined in air at 550 °C for 12 h. A heating rate of 2 °C min^{-1} was applied.

Table 1. Argon sorption and SAXS data of SBA-15 and transformed materials. The data of a mechanical mixture of SBA-15 and MCM-41 are shown for comparison.

Sample	d_{DFT} / nm	V_{tot} / cm^3 g^{-1}	a_0 (large) / nm	a_0 (small) / nm	m_{silica} / m_{NaOH}
SBA-15	7.1	0.68	10.3	–	–
SBA-15 T1	6.6, 4.0	0.66	10.1	–	15
SBA-15 T2	6.1, 4.1	0.46	9.8	–	12
SBA-15 T3	4.0	0.63	9.7	4.3	6
SBA-15/MCM-41	7.1, 3.7	0.61	10.3	4.3	–

Table 2. Argon sorption and SAXS data of SBA-16 and transformed materials. The data of a mechanical mixture of SBA-16 and MCM-41 are shown for comparison.

Sample	d_{DFT} / nm	V_{tot} / $cm^3\ g^{-1}$	a_0 (large) / nm	a_0 (small) / nm	m_{silica} / m_{NaOH}
SBA-16	6.2	0.70	13.4	–	–
SBA-16 T1	6.4, 4.6	0.44	13.2	–	13
SBA-16 T2	5.5, 3.8	0.50	13.0	–	11
SBA-16 T3	4.0	0.48	13.0	5.2	9
SBA-16/MCM-41	6.2, 3.8	0.26	13.4	4.4	–

2.6. Physical Measurements

Argon sorption isotherms (54 measurement points for adsorption, 40 points for desorption) were measured at 87.3 K with a Quantachrome Autosorb iQ MP equipped with a CryoCooler. Pore size distributions and average pore diameters d_{DFT} were determined from the adsorption isotherms (unless indicated otherwise) by a non-local density functional theory (NLDFT) model developed for silica exhibiting cylindrical pore geometry (Software ASiQwin v3.01, Quantachrome Instruments) [21]. For the parent SBA-16, a kernel for spherical cavities was used. Total pore volumes V_{tot} were derived from the amount of adsorbed argon at a relative pressure of p/p_0 = 0.95. Scanning electron microscopy (SEM) images were collected with a FEI Quanta FEG 250. SAXS patterns were recorded on a Bruker NanoStar in transmission mode with Cu$K\alpha_1$ radiation.

3. Results and Discussion

3.1. General Considerations

The pseudomorphic transformation of mesoporous silica particles in the presence of a SDA is governed by the processes of dissolution and precipitation. The rate of dissolution/precipitation thereby depends on various parameters, including pH, temperature, and solvent [17,22]. The particle morphology remains intact upon transformation, whereas the pore structure can undergo a rearrangement. Figure 1 compares SEM images of SBA-15 and SBA-16 before and after pseudomorphic transformation. The agglomerated submicrometer-sized primary SBA-15 particles are retained upon transformation, whereas the transformed SBA-16 sample features the typical micrometer-sized cubic particles of the parent SBA-16.

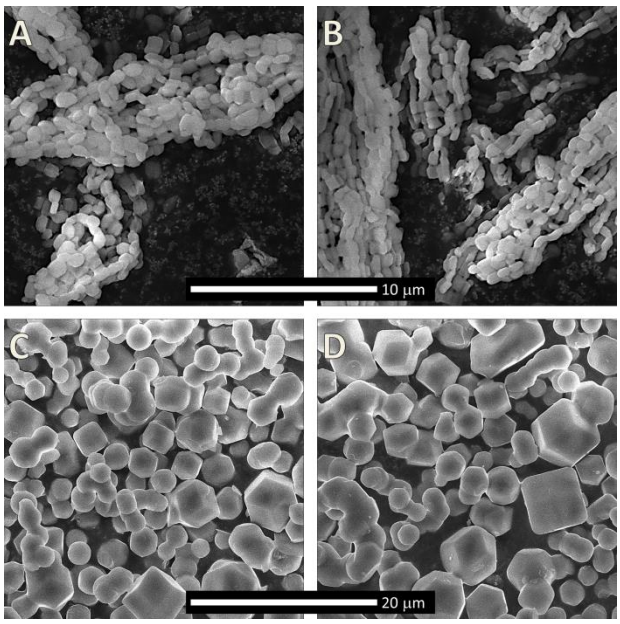

Figure 1. SEM images of parent SBA-15 (A), SBA-15 T3 (B), parent SBA-16 (C), and SBA-16 T3 (D). Note the unaltered particle morphology after transformation.

The dissolution and reprecipitation of the silicate species at high pH generates a modified pore structure with a reduced pore diameter, the value of which is determined by the SDA [14]. Starting with SBA-15 or SBA-16 parent materials and adjusting the silica/NaOH ratio, we have investigated three degrees of pseudomorphic transformation, namely a low (T1), intermediate (T2), and high degree (T3) of transformation. Argon sorption and SAXS were used to analyze the structural changes upon transformation. Key properties of the samples under investigation are summarized in Tables 1 and 2.

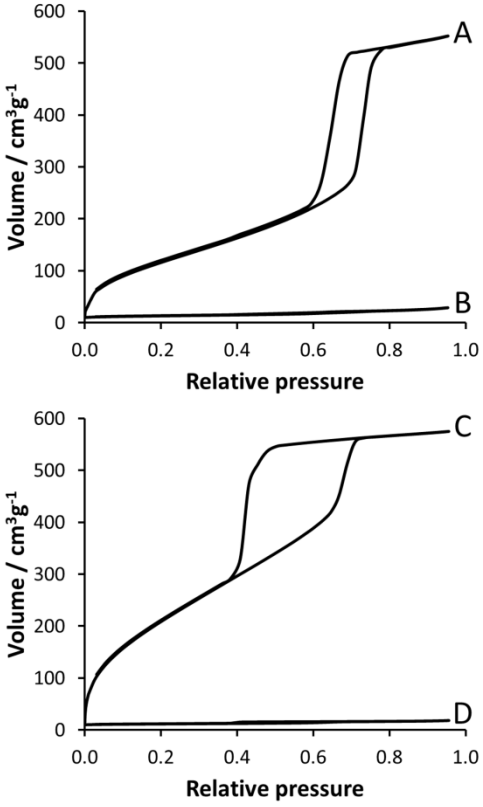

Figure 2. Top: Argon sorption isotherms of SBA-15 before (A) and after (B) uptake of SDA. Bottom: Argon sorption isotherms of SBA-16 before (C) and after (D) uptake of SDA. The samples were dried for 16 h at 80 °C before the measurement.

A prerequisite for a pseudomorphic transformation in the presence of a SDA, is the introduction of the SDA into the pores of the parent material. The sorption isotherms shown in Figure 2 were measured before the hydrothermal treatment of the samples, i.e., after stirring of the parent materials in an alkaline aqueous solution of CTAB for 30 min. Comparison with the respective untreated parent materials reveals a significantly reduced argon sorption capacity due to the presence of the SDA in the pores.

3.2. Transformation of SBA-15

Particles with two well-defined mesopore domains can be prepared by a partial pseudomorphic transformation of SBA-15 [18]. Argon sorption isotherms of the SBA-15 parent material and of the pseudomorphically transformed materials with various degrees of transformation are shown in Figure 3. As expected, the parent SBA-15 shows a H1 hysteresis [23] and a relatively narrow pore size distribution centered at 7.1 nm. A tail extending to 3.5 nm is indicative of the small intrawall mesopores that are created by the hydrophilic poly(ethylene oxide) segments of the non-ionic block copolymer SDA during hydrothermal treatment [24,25]. After transformation in the presence of CTAB, a second pore condensation step appears in the adsorption isotherm at lower relative pressure (p/p_0 = 0.38). This additional pore condensation step is caused by the newly formed domains with an average pore size of 4 nm.

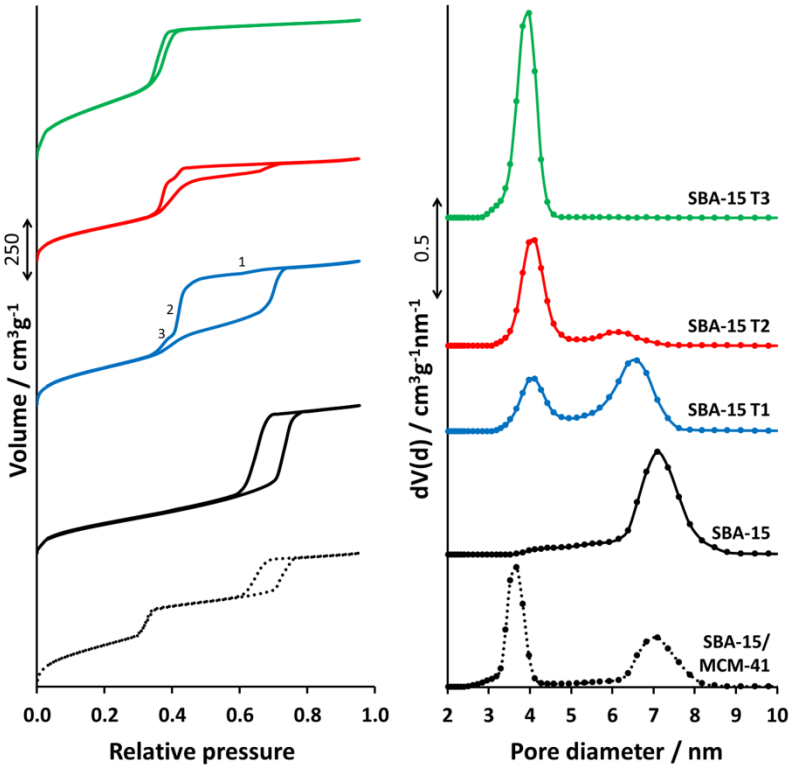

Figure 3. Argon sorption isotherms (left) and corresponding pore size distributions (right) of a mechanical mixture of SBA-15 and MCM-41, parent SBA-15, and the transformed materials SBA-15 with various degrees of transformation (T1 to T3). The isotherms and pore size distributions are offset for clarity.

The desorption isotherms of the partially transformed SBA-15 are complex and, in agreement with previously reported results from nitrogen sorption [18], consist of three segments, as is best seen in the desorption isotherm of SBA-15 T1 (Figure 3). Starting from high relative pressure, the first step in the desorption isotherm corresponds to evaporation from unobstructed SBA-15 pores (step 1), followed by a step at $p/p_0 = 0.41$ (step 2) and a subsequent smaller step (step 3) leading to the closure of the hysteresis loop at $p/p_0 = 0.36$. If we assume a structure where the large pores (6.6 nm) are interconnected with the small pores (4.0 nm), steps 2 and 3 can be assigned to cavitation followed by evaporation of argon from

the small pores (or necks). Cavitation implies the spontaneous nucleation and growth of gas bubbles in the metastable condensed fluid present in the large pores (or cavities), while the fluid in the small pores (or necks) remains in a stable state. For argon at 87.3 K in cylindrical pores, a critical neck size of approximately 5 nm has been proposed [26]. Below this critical neck size, desorption is generally assumed to occur by cavitation [27]. Due to the comparatively small neck size in SBA-15 T1, it is very likely that cavitation is the cause for the unusual desorption isotherms of the partially transformed materials.

The type of evaporation mechanism can be determined by measuring the sorption isotherms with different adsorptives, e.g., nitrogen and argon [28]. If evaporation occurs by cavitation, the relative pressure of evaporation does not correlate with the neck size. The pore size distribution calculated from the desorption isotherm should therefore yield different pore size values for nitrogen and argon. If the pore size distributions calculated from these desorption isotherms are similar, evaporation follows a pore blocking mechanism and the neck size can be directly determined from the desorption isotherm. Figure 4 compares the argon and nitrogen sorption isotherms of SBA-15 T1 and the pore size distributions calculated from the respective desorption isotherm, yielding an “artificial” average pore size of 4.4 nm (argon) and 5.1 nm (nitrogen). Calculations of the pore sizes based on the adsorption isotherms yield identical results independent of whether argon or nitrogen is used as an adsorptive. This confirms that step 2 in the desorption isotherm of SBA-15 T1 is caused by cavitation.

The adsorption and desorption isotherms of SBA-15 T2 feature the same steps as observed for SBA-15 T1, with the major adsorption/desorption processes now being associated with the small pores. SBA-15 T3 shows a type IV(a) isotherm [23], which leads us to the conclusion that regarding the pore size of the material, transformation to a pore system with a smaller pore size is complete.

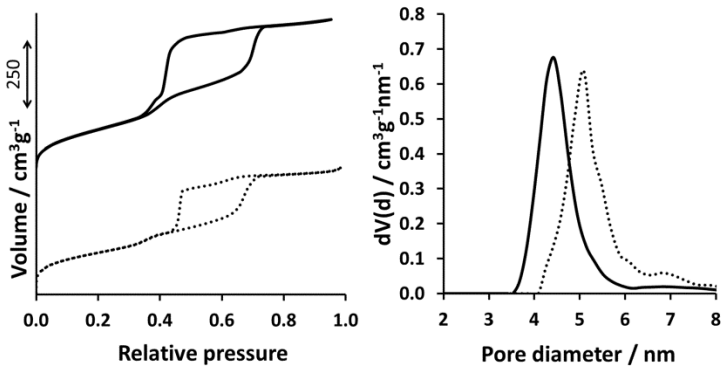

Figure 4. Argon sorption (87.3 K, solid line) and nitrogen sorption (77 K, dotted line) isotherms of SBA-15 T1. The isotherms are offset for clarity. The pore size distributions calculated from the respective desorption isotherms are shown on the right.

A comparison of the argon sorption isotherms of the transformed materials with the isotherms of a mechanical mixture of SBA-15 and MCM-41 supports the assumption of interconnected large mesopore and small mesopore domains in the case of the partially transformed samples, although we cannot exclude that some of the small pores in the partially transformed samples SBA-15 T1 and SBA-15 T2 are present as isolated domains that are not interconnected with the large pore domains. It is interesting to note that the pore size of the original SBA-15 domain decreases with increasing degree of transformation until it disappears from the pore size distribution at a high degree of transformation (SBA-15 T3).

SAXS provides additional information on the newly introduced pore structures. The SAXS patterns of the parent and transformed SBA-15 samples are shown in Figure 5. The repeat distances a_0 of the small and large mesopore domains are given in Table 1. All samples feature the typical (100), (110), and (200) peaks, representative of the hexagonal space group $P6mm$ [3]. With increasing degree of transformation, the intensity of the (100) peak decreases. This can be attributed to a degradation of the mesoscopic pore ordering of the parent SBA-15. Small pore domains form close to the external particle

surface, whereas the pore diameter of the parent SBA-15 domains is slightly reduced. Normalizing the patterns to the (100) peak of the SBA-15 domains reveals the development of the small pore domains (Figure 5, right). While these newly formed domains are not clearly distinguishable in the SAXS patterns of SBA-15 T1 and SBA-15 T2, sample SBA-15 T3 shows a pattern that can be assigned to two different phases, namely the hexagonal SBA-15 phase ((100), (110), and (200)) and a newly formed hexagonal phase ((100*), (110*), and (200*)) with shorter repeat distance a_0. This new hexagonal phase is related to a classical MCM-41 type pore structure. A comparison of the SBA-15 T3 pattern with the pattern of a mechanical mixture of SBA-15 and MCM-41 illustrates the matching peaks (Figure 6).

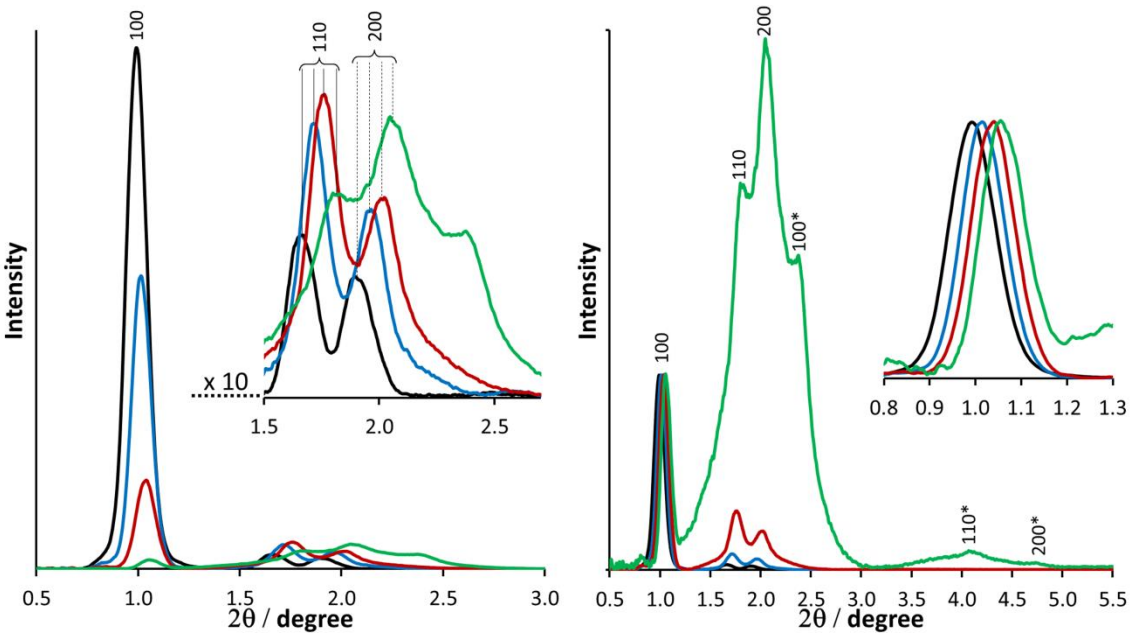

Figure 5. Left: SAXS patterns of parent SBA-15 (black), SBA-15 T1 (blue), SBA-15 T2 (red), and SBA-15 T3 (green). Right: SAXS patterns of the same samples normalized to the (100) peak. The inset shows the shift of the (100) peak with increasing degree of transformation.

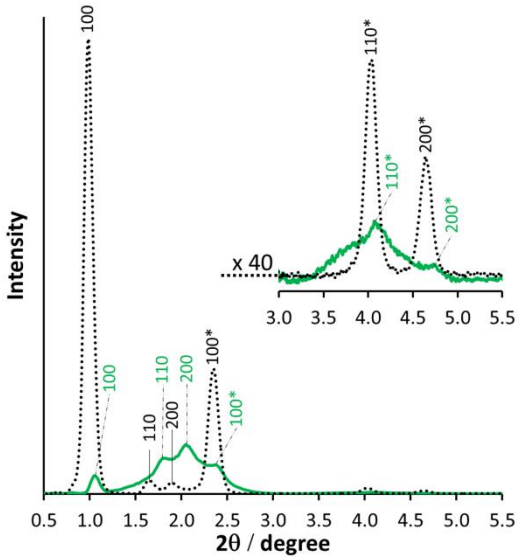

Figure 6. SAXS patterns of a mechanical mixture of SBA-15 and MCM-41 (dotted line) and SBA-15 T3 (green line).

Based on the analysis of the argon sorption isotherms, we initially assumed that the sample SBA-15 T3 was fully transformed, as the respective pore size distribution no longer showed contributions of the parent SBA-15 (Figure 3). However, the SAXS pattern of SBA-15 T3 still provides evidence for the presence of a structure with a SBA-15 type pore spacing (Figure 6). Taking the pore size distribution into consideration, we can conclude that some of the original SBA-15 pores (7.1 nm) have been transformed into smaller pores (4.0 nm) while retaining their original pore spacing.

From these results and previous studies on the accessibility of the large pore domains in partially transformed SBA-15 samples [18], the pseudomorphic transformation of SBA-15 can be described by a process that replaces the SBA-15 pore system close to the external particle surface with MCM-41 type domains, leading to the formation of bottlenecks. A higher degree of transformation can be achieved by

decreasing the silica/NaOH ratio. This not only promotes the formation of the small pore domains, but also reduces the pore size of the SBA-15 domains while retaining the original pore spacing. A schematic representation of the transformed pore structures is given in Figure 7.

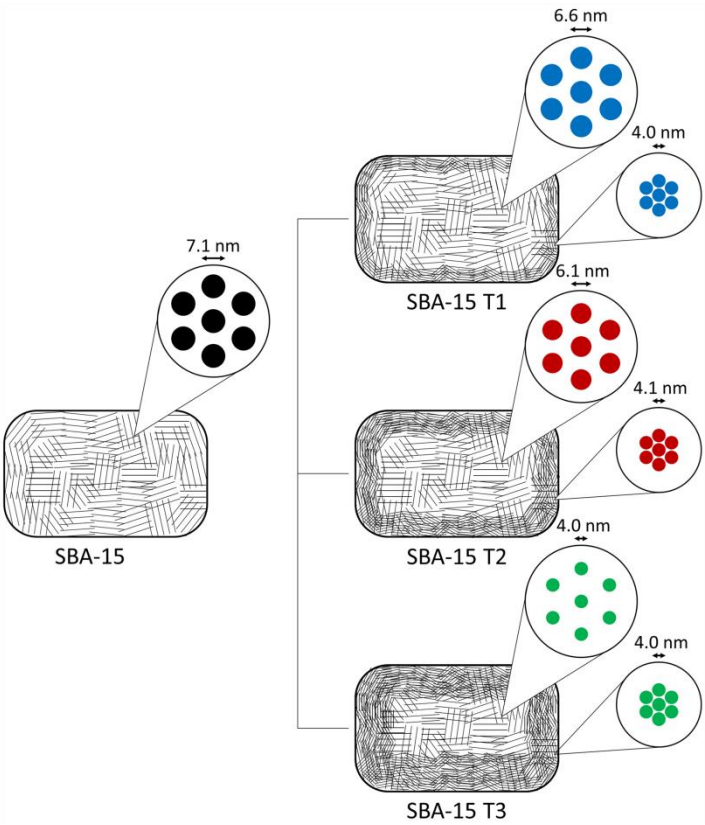

Figure 7. Schematic representation of the pore structure domains obtained after various degrees of transformation.

The pore wall thickness of an ordered mesoporous material can be obtained by subtracting the pore diameter from the repeat distance. Application of this concept to SBA-15 T3 yields a pore wall thickness of 0.3 nm, which is substantially smaller than values obtained for typical MCM-41 materials [29].

However, it should be kept in mind that the small repeat distance is calculated from the SAXS peaks of the MCM-41 type domains, whereas the pore size distribution contains an additional contribution from the domains with SBA-15 type pore spacing, which could feature a slightly larger pore size.

3.3. Transformation of SBA-16

The structure of SBA-16 is characterized by a three-dimensional network of cage-like pores, which are arranged in a body-centered-cubic array and connected through small mesopores [30,31]. The argon sorption isotherm of SBA-16 (Figure 8) features a large hysteresis loop, typical for materials with ink-bottle pores [28]. The desorption branch of the hysteresis loop is steeper than the adsorption branch, leading essentially to a H2(a) hysteresis [23]. Close inspection of the desorption isotherm reveals two segments, with the lower pressure segment being steeper, thus indicating a forced closure of the hysteresis loop. This forced closure occurs at a relative pressure of p/p_0 = 0.40 and thus at a higher relative pressure than the lower closure point observed in the case of cylindrical pores (p/p_0 = 0.36). This is in agreement with previous reports on adsorption hysteresis in ink-bottle type pores, where it was found that the pressure of cavitation in spherical pores is slightly higher than the lower closure point of the hysteresis loop in materials with cylindrical pores [26]. The pore size distribution of SBA-16 shows a narrow peak at 6.2 nm and a broad contribution extending from 1.8 to 5.3 nm. The latter can be attributed to the non-uniformity of the micro- and mesopores that are often observed in materials prepared with $EO_xPO_yEO_x$ block copolymer templates [31].

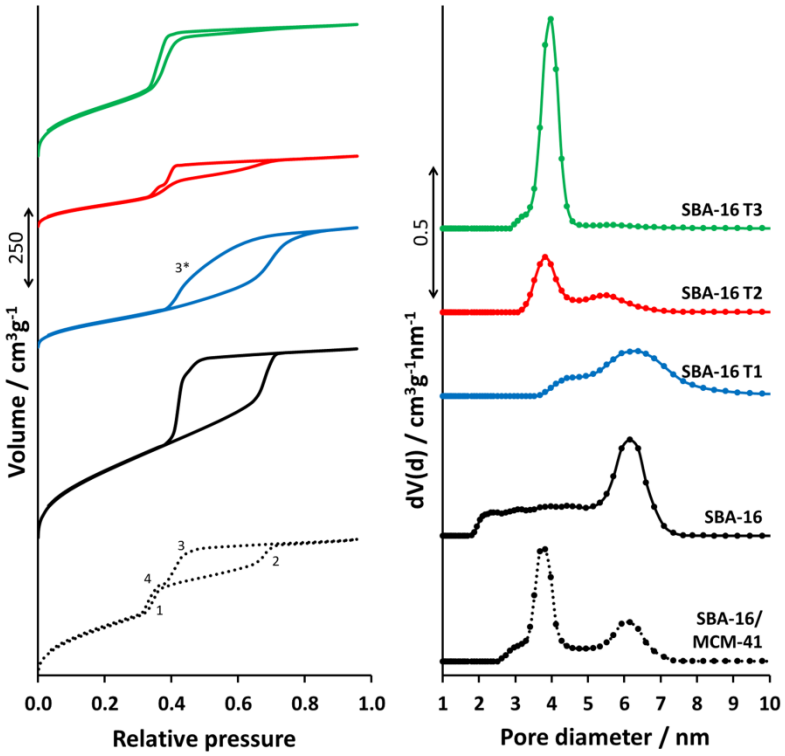

Figure 8. Argon sorption isotherms (left) and corresponding pore size distributions (right) of a mechanical mixture of SBA-16 and MCM-41, parent SBA-16, and the transformed materials SBA-16 with various degrees of transformation (T1 to T3). The isotherms and pore size distributions are offset for clarity.

After partial pseudomorphic transformation (SBA-16 T1) a H2(b) hysteresis is observed. The H2(b) loop is typically associated with pore blocking and a wide distribution of neck sizes [23]. Contrary to the desorption isotherm of the parent SBA-16, the desorption isotherm of SBA-16 T1 decreases gradually with a slight step (3*, Figure 8) before closing at p/p_0 = 0.40. Transformation apparently leads to an enlargement of the pore necks and a broadening of the neck size distribution. The pore size distribution of SBA-16 T1 confirms the elimination of pores with a diameter below 3.8 nm.

At a higher transformation degree (SBA-16 T2), two adsorption steps can be distinguished. These steps correspond to the two steps observed in the adsorption isotherm of the SBA-16/MCM-41 mixture (steps 1 and 2, Figure 8), indicating the partial transformation of the SBA-16 pore structure and the introduction of small pore domains. The respective pore size distribution shows maxima at 3.8 and 5.5 nm. The desorption isotherm of SBA-16 T2 features a step at $p/p_0 = 0.38$, which we assign to cavitation. Note that compared to the parent SBA-16 the cavitation step has shifted to lower relative pressure. A possible interpretation is the transformation of the original pore structure with spherical cavities into a structure with pores approaching a cylindrical shape.

The pore size distribution and isotherms of SBA-16 T3 contain only minor contributions of the parent pore size and thus point to an almost complete transformation. The question remains whether the newly introduced pore structure corresponds to an actual MCM-41 type phase with a hexagonal pore arrangement. SAXS patterns of the samples are shown in Figure 9. Similar to the transformation of SBA-15, a decrease of the main peak (110) is observed upon increasing the degree of transformation, accompanied by a slight shift to larger angles. Interestingly, an increasing intensity is observed in the 2θ range between 1.2 and 3.0°, suggesting the formation of a new framework. Comparison with the SAXS pattern of a mechanical mixture of SBA-16 and MCM-41 (Figure 10) points to the presence of a hexagonal phase ((100*), (110*), (200*)) and of a cubic phase ((110), (200), (211), (220)).

Comparing the SAXS pattern of a mechanical mixture of SBA-16 and MCM-41 with the pattern of SBA-16 T3 provides evidence for the conservation of the cubic structure (Figure 10), despite the observation that the pore size distribution of SBA-16 T3 (Figure 8) shows only a minor contribution of the parent pore size. Similar results were obtained when decreasing the silica/NaOH ratio to 7. The pore structure of the transformed SBA-16 can thus be described by means of a hybrid structure consisting of domains with one-dimensional pores and domains with a three-dimensional pore system originating from the parent

SBA-16, but with reduced pore size. It is likely that the cavities of SBA-16 have been transformed into a cubic network of cylindrical channels. The SAXS peaks that can be assigned to the hexagonal domains formed upon transformation are comparatively broad and therefore indicative of poor long-range ordering.

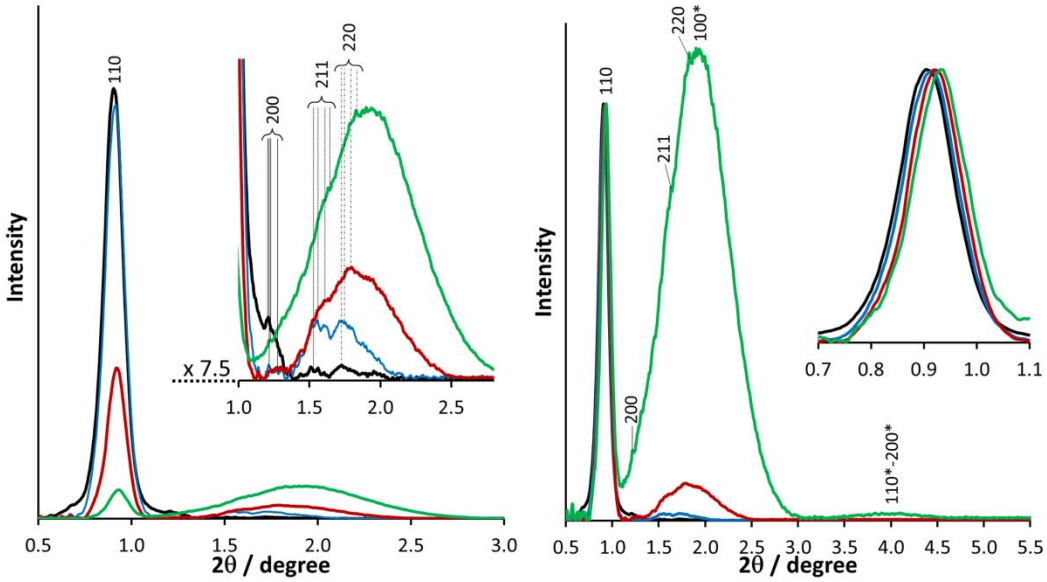

Figure 9. Left: SAXS patterns of parent SBA-16 (black), SBA-16 T1 (blue), SBA-16 T2 (red), and SBA-16 T3 (green). Right: SAXS patterns of the same samples normalized to the (110) peak. The inset shows the shift of the (110) peak with increasing degree of transformation.

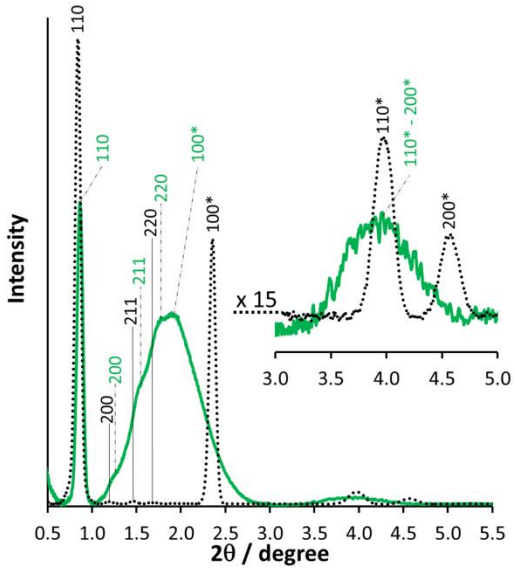

Figure 10. SAXS patterns of a mechanical mixture of SBA-16 and MCM-41 (dotted line) and SBA-16 T3 (green line).

4. Conclusions

The pseudomorphic transformation of ordered mesoporous silica yields materials with hybrid pore structures. The analysis of the transformed samples by SAXS shows that structural features of the starting material are retained upon transformation, even at high transformation degree where a seemingly complete conversion of large to small pores is obtained. The pore structure of the starting material therefore determines to a certain extent the pore structure of the transformed material. The characteristically large pore spacing of SBA-15 is still found in the transformed material, although the pore size has been significantly reduced. Similarly, a cubic phase is observed in the SAXS patterns of materials obtained by pseudomorphic transformation of SBA-16.

Pseudomorphic transformation can be used on any porous silica, as long as an efficient uptake of the SDA is possible. We have shown that even in the case of SBA-16 with its relatively narrow pore necks, the

pores can be filled with hexadecyltrimethylammonium ions. Due to the particle shape being unaltered after transformation, the pathway of pseudomorphic transformation implies less compromise between pore structure and particle shape, in particular when compared to classical mesoporous silica syntheses.

The ability to design complex pore structures, such as cylindrical pores with bottlenecks, is essential for advancing the understanding of gas sorption isotherms. Adsorption-desorption hysteresis can provide valuable information on pore connectivity, bottlenecks, and cavities. The well-defined structural features of a pseudomorphically transformed material are an ideal basis for studying evaporation mechanisms such as cavitation and pore blocking.

Acknowledgements

Financial support by the Swiss National Science Foundation (projects 200021_149715 and 200021_172805) is acknowledged.

References

[1] C. T. Kresge, M. E. Leonowicz, W. J. Roth, J. C. Vartuli, J. S. Beck, Nature 359 (1992) 710-712.

[2] J. S. Beck, J. C. Vartuli, W. J. Roth, M. E. Leonowicz, C. T. Kresge, K. D. Schmitt, C. T.-W. Chu, D. H. Olson, E. W. Sheppard, S. B. McCullen, J. B. Higgins, J. L. Schlenker, J. Am. Chem. Soc. 114 (1992) 10834-10843.

[3] D. Zhao, Q. Huo, J. Feng, B. F. Chmelka, G. D. Stucky, J. Am. Chem. Soc. 120 (1998) 6024-6036.

[4] D. Zhao, J. Feng, Q. Huo, N. Melosh, G. H. Fredrickson, B. F. Chmelka, G. D. Stucky, Science 279 (1998) 548-552.

[5] T. Cheng, Q. Zhao, D. Zhang, G. Liu, Green Chem. 17 (2015) 2100-2122.

[6] I. Sierra, D. Pérez-Quintanilla, S. Morante, J. Gañán, J. Chromatogr. A 1363 (2014) 27-40.

[7] M. Sohmiya, K. Saito, M. Ogawa, Sci. Technol. Adv. Mater. 16 (2015) 1-17.

[8] X. Qian, K. Fuku, Y. Kuwahara, T. Kamegawa, K. Mori, H. Yamashita, ChemSusChem 7 (2014) 1528-1536.

[9] A. F. Moreira, D. R. Dias, I. J. Correia, Microporous Mesoporous Mater. 236 (2016) 141-157.

[10] F. Hoffmann, M. Cornelius, J. Morell, M. Fröba, Angew. Chem. Int. Ed. 45 (2006) 3216-3251.

[11] D. Brühwiler, Nanoscale 2 (2010) 887-892.

[12] B. Albela, L. Bonneviot, New J. Chem. 40 (2016) 4115-4131.

[13] T. Martin, A. Galarneau, F. Di Renzo, F. Fajula, D. Plee, Angew. Chem. Int. Ed. 41 (2002) 2590-2592.

[14] M. J. Reber, D. Brühwiler, Part. Part. Syst. Charact. 32 (2015) 243-250.

[15] J. Patzsch, J. J. Schneider, Dalton Trans. 42 (2013) 1451-1460.

[16] G.-T. Zhu, X.-S. Li, Q. Gao, N.-W. Zhao, B.-F. Yuan, Y.-Q. Feng, J. Chromatogr. A 1224 (2012) 11-18.

[17] X. Li, D. Wu, J. Wang, W. Zhu, Y. Luo, C. Han, W. Ma, S. He, Microporous Mesoporous Mater. 226 (2016) 309-315.

[18] M. J. Reber, D. Brühwiler, Dalton Trans. 44 (2015) 17960-17967.

[19] D. Brühwiler, H. Frei, J. Phys. Chem. B 107 (2003) 8547-8556.

[20] M. Mesa, L. Sierra, J. Patarin, J.-L. Guth, Solid State Sci. 7 (2005) 990-997.

[21] J. Landers, G. Y. Gor, A. V. Neimark, Colloids Surf. A 437 (2013) 3-32.

[22] W. C. Yoo, A. Stein, Chem. Mater. 23 (2011) 1761-1767.

[23] M. Thommes, K. Kaneko, A. V. Neimark, J. P. Olivier, F. Rodriguez-Reinoso, J. Rouquerol, K. W. Sing, Pure Appl. Chem. 87 (2015) 1051-1069.

[24] R. Ryoo, C. H. Ko, M. Kruk, V. Antochshuk, M. Jaroniec, J. Phys. Chem. B 104 (2000) 11465-11471.

[25] A. Galarneau, H. Cambon, F. Di Renzo, R. Ryoo, M. Choi, F. Fajula, New J. Chem. 27 (2003) 73-79.

[26] P. I. Ravikovitch, A. V. Neimark, Langmuir 18 (2002) 9830-9837.

[27] C. J. Rasmussen, A. Vishnyakov, M. Thommes, B. M. Smarsly, F. Kleitz, A. V. Neimark, Langmuir 26 (2010) 10147-10157.

[28] M. Thommes, B. Smarsly, M. Groenewolt, P. I. Ravikovitch, A. V. Neimark, Langmuir 22 (2006) 756-764.

[29] M. Kruk, M. Jaroniec, Y. Sakamoto, O. Terasaki, R. Ryoo, C. H. Ko, J. Phys. Chem. B 104 (2000) 292-301.

[30] Y. Sakamoto, M. Kaneda, O. Terasaki, D. Y. Zhao, J. M. Kim, G. Stucky, H. J. Shin, R. Ryoo, Nature 408 (2000) 449-453.

[31] K. Miyasaka, H. Hano, Y. Kubota, Y. Lin, R. Ryoo, M. Takata, S. Kitagawa, A. V. Neimark, O. Terasaki, Chem. Eur. J. 18 (2012) 10300-10311.